Electronic Supplementary Material (ESI) for Nanoscale.

Electronic Supporting Information for:

Lamellar nanoporous gold thin films with tunable porosity for ultrasensitive SERS detection in liquid and gas phase

Adrien Chauvin,[a,b] Marta Lafuente,[c,d] Jean Yves Mevellec,[a] Reyes Mallada,[c,d] Bernard Humbert,[a] Maria Pilar Pina,[c,d] Pierre Yves Tessier [a]* and Abdelaziz El Mel [a]

[a] Institut des Matériaux Jean Rouxel, IMN, Université de Nantes, CNRS, 2 rue de la Houssinière B.P. 32229, 44322 Nantes cedex 3, France.

[b] Department of Condensed Matter Physics, Faculty of Mathematics and Physics, Charles University, Ke Karlovu 5, 121 16 Praha 2, Czech Republic.

[c] Instituto de Nanociencia de Aragón (INA). Campus Rio Ebro, Universidad de Zaragoza, C/Mariano Esquillor, s/n, 50018 Zaragoza, Spain.

[d] Instituto de Ciencia de Materiales de Aragón (ICMA), Universidad de Zaragoza-CSIC, 50009 Zaragoza, Spain.

Corresponding authors: pierre-yves.tessier@cnrs-imn.fr

Table of contents

ESI. 1: TEM initial cross section analysis

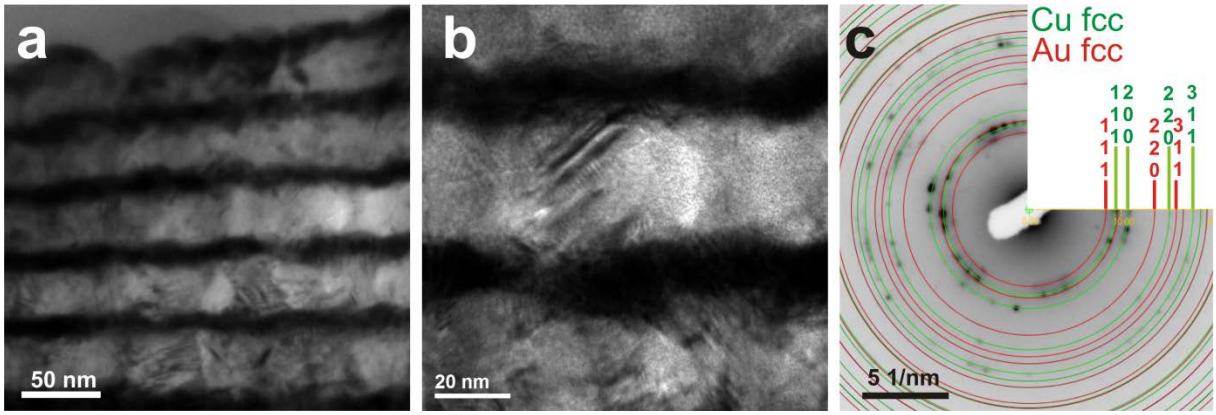

Fig. S1 TEM cross section images in low (a) and (b) high magnification of the stacked structure after deposition of 8 nm of gold and 30 nm of copper on PET substrate. On TEM cross section images the stacked structure can be easily seen with the wavy structure observed by SEM analysis. (c) An electron diffraction analysis is also performed on this sample.

The associated selected-area electron diffraction pattern indexed according to the crystallographic database of face centered cubic gold and copper. The corresponding diffraction pattern shows the polycrystalline nature of the layer. This analysis confirms the lack of crystalline phase of Au-Cu alloy in this sample. Transmission electron microscopy (TEM) and selected area electron diffraction (SAED) are performed on a Hitachi H9000-NAR microscope (LaB_6 filament, 300 kV, Scherzer resolution: 0.18 nm). For these TEM analysis, the initial stacked structure are deposited on PET substrate, then sliced with ultra-microtome and deposited on a carbon coated nickel TEM grid.

ESI.2: Study of the SERS performance of nanoporous gold

For the study of SERS performance of nanoporous gold, bipyridine solution at 10^{-3} mol.L^{-1} is also used with the same process reported in the main paper. The synthesis of the nanoporous gold is realized according to the process described by El Mel et al.[1] Briefly, this process involved the magnetron cosputtering deposition of gold copper (500 nm thick) alloy followed by dealloying in nitric acid at 16 mol.L^{-1}. The study of SERS performance is realized on three initial gold concentration (16, 24 and 32 at.%) dealloyed during 25, 60, 120, 300 min.

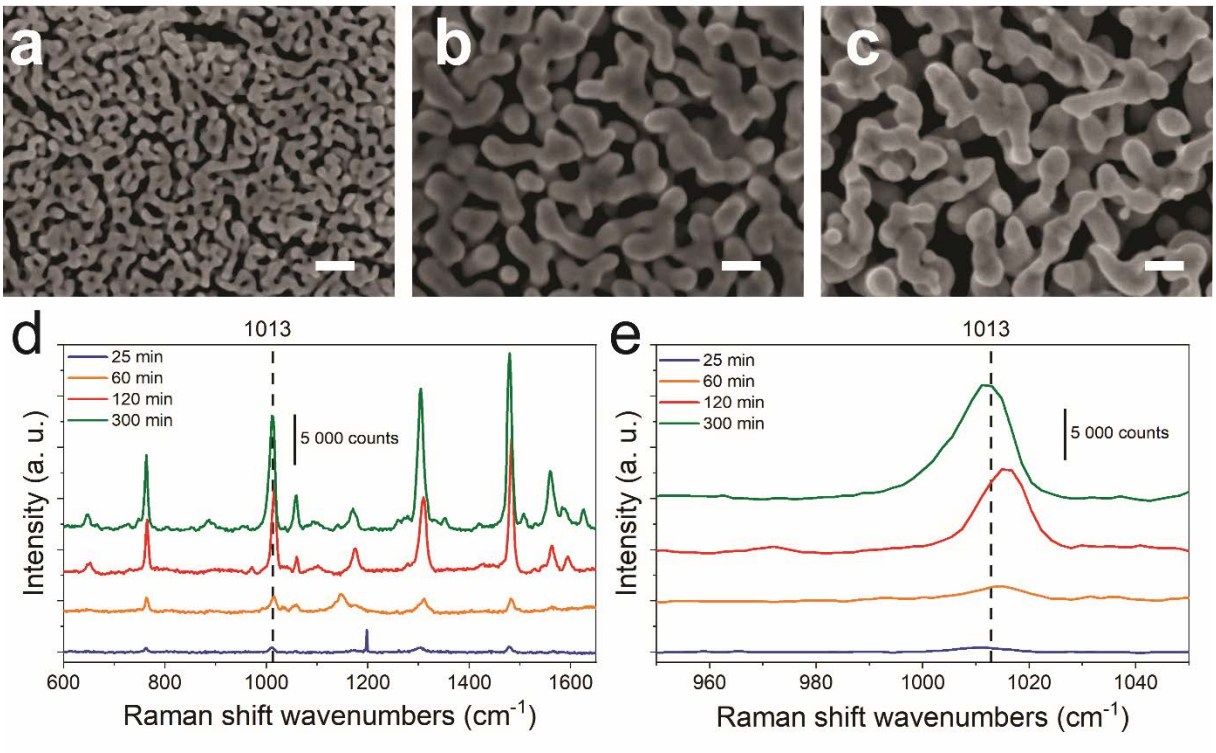

Fig. S2 Study of the Raman intensity of bypiridine soak on nanoporous gold sample obtained with an initial gold content of 16 at.% and dealloyed during different times. (a-c) Typical plan view SEM images of the sample dealloyed in nitric acid at 16 mol.L^{-1} during (a) 25 min, (b) 60 min and (c) 300 min. (d) Raman spectra of sample after 24 h immersion in 10^{-3} mol.L^{-1} solution of bipyridine for sample with 16 at.% of gold at initial state and dealloyed during different time: (blue) 25, (orange) 60, (red) 120 and (green) 300 min with (e) a zoom on the peak at 1013 cm^{-1}.

For sample dealloyed during 25 min, a weak Raman signal of the molecule can be observed. When the dealloying time increases at 60 min, a higher Raman signal is shown with a shift of the peak for high wavelength number. This shift can be due to the modification of the conformation of the molecule during the analysis. Finally, when the dealloying time reaches 120 and 300 min, the intensity at 1013 cm^{-1} is the highest.

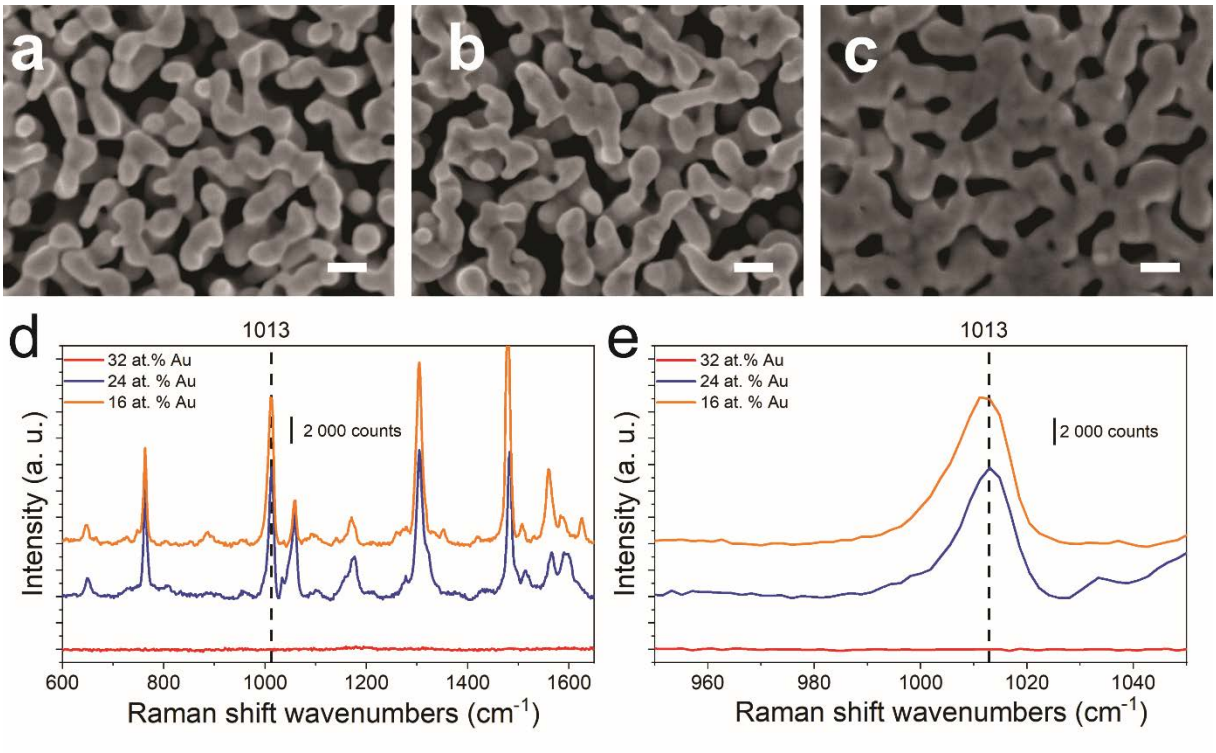

Fig. S3 Study of the Raman intensity of the bypiridine soak on nanoporous gold sample obtained with different initial gold content and dealloyed during 300 min. (a-c) Typical plan view SEM images of nanoporous gold dealloyed during 300 min with (a) 16, (b) 24 and (c) 32 at.% of gold at initial state. (d) Raman spectra of a sample after 24 h in 10^{-3} mol.L^{-1} solution of bipyridine for a sample with different gold content at initial state: (orange) 16, (blue) 24 and (red) 32 at.% dealloyed during 300 min with (e) a zoom on the pic at 1013 cm^{-1}.

For an initial gold content of 16 at.%, the Raman signal is the highest observed. When increasing the initial gold content to 24 at.%, a small decrease of the intensity is shown. Finally, when the initial gold content reaches 32 at.%, the Raman signal of bipyridine disappears. The decrease of the signal can originate from the global morphology of the sample after dealloying. Sample with 16 at.% of gold at initial state and dealloyed during 300 min is constituted of interconnected nanoligaments with a pore size around 75 nm and sample with 32 at.% of gold at initial state dealloyed during 300 min show thicker nanoligaments with smaller pore size (≈ 60 nm). The number of hot spots is higher for samples with small nanoligaments. In nanoporous structure, the main enhancement effect originate from the high positive curvature of nanopores.[2,3] However, in the case of small ligament the main enhancement are created between two adjacent ligament.[4] In this second case, the Raman enhancement is much more intense.[5,6] Therefore, structure with the lowest ligament size have higher Raman signal enhancement. Afterward, for the study of the detection limit, sample with an initial gold content of 24 and 16 at.% at initial state dealloyed during 300 min are selected.

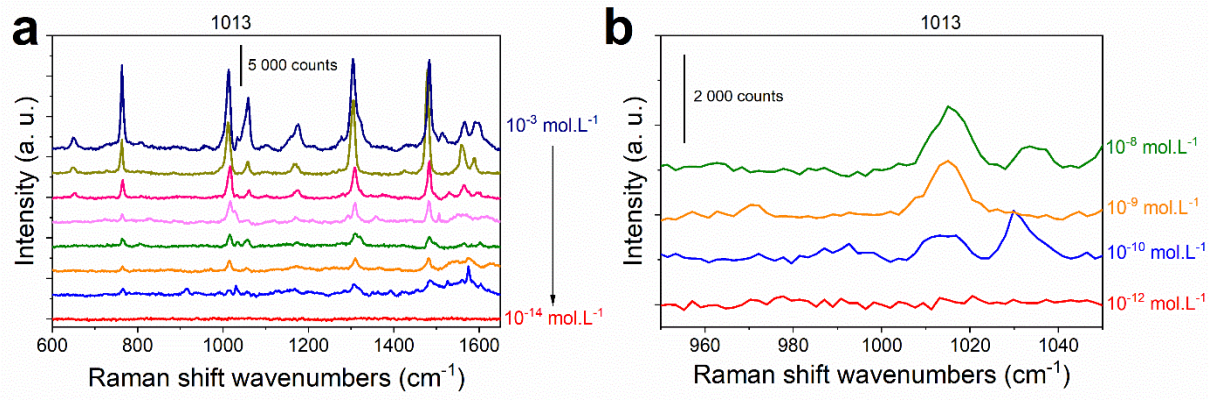

Fig. S4 Detection limit for nanoporous gold. (a) Raman spectra of a sample with 24 at.% gold at initial state and dealloyed during 300 min after 24 h in different concentration of bipyridine solution with a (b) zoom on the pic at 1013 cm^{-1}. A clear decrease of the signal can be observed until 10^{-10} $mol.L^{-1}$. For a bipyridine concentration of 10^{-12} $mol.L^{-1}$, no signal is observed. The detection limit for this nanoporous gold with an initial gold content of 24 at.% is between 10^{-10} $mol.L^{-1}$ and 10^{-12} $mol.L^{-1}$.

ESI.3: Method for morphological data collection

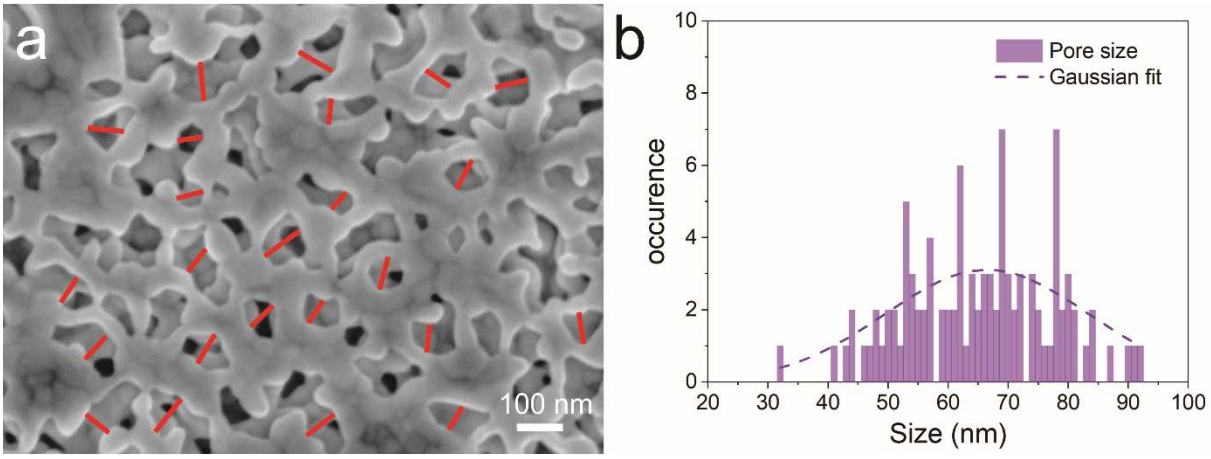

Fig. S5 Pore size estimation from top view SEM images. The illustrative example reported here corresponds to the sample with an initial gold layer of 8 nm and an initial copper layer of 90 nm etched during 300 min. This methodology is used for all samples reported in the paper. First, for the size of the pore, a manual collection is used on the plan view SEM images. (a) A batch of 100 measurements is collected for each sample (red line in the figure corresponds to some collected measurements). (b) The resulting dispersion shows a Gaussian trend with a high dispersion of measurement high lightening the wide dispersion of the pore size. Values reported in the paper correspond to the center of the Gaussian curve.

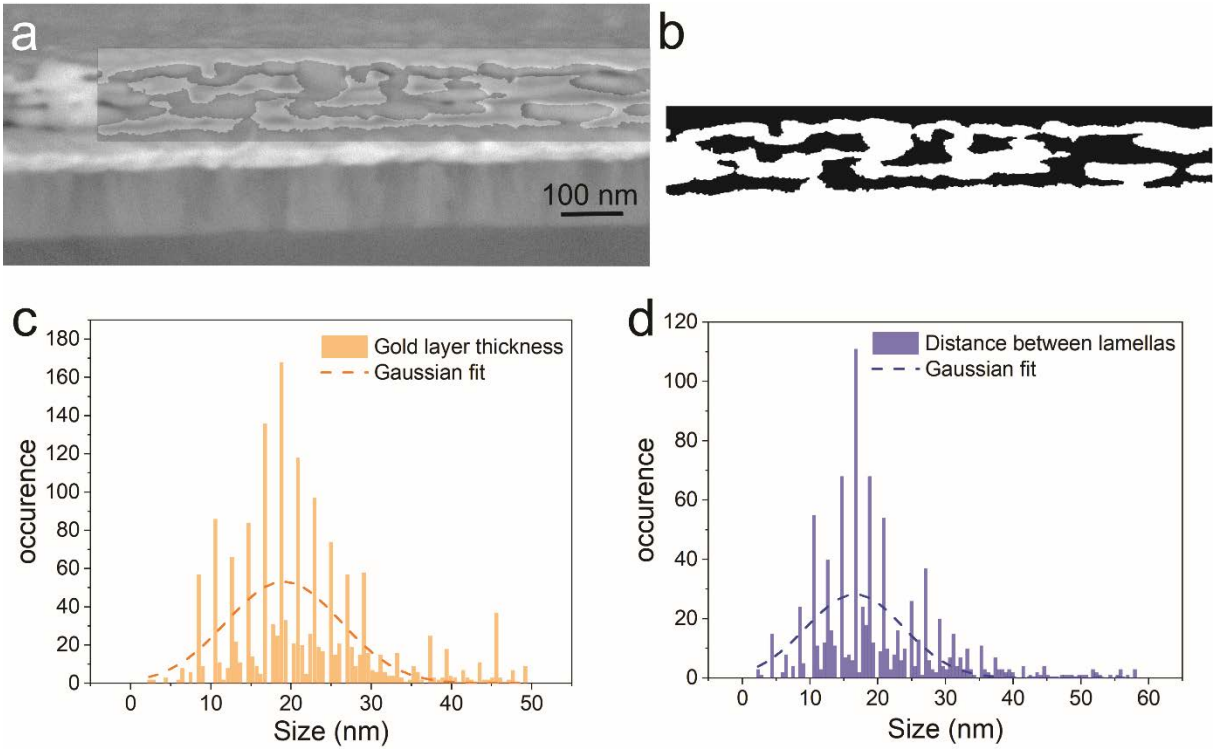

Fig. S6 Estimation of thickness and interspacing of Au lamellas from cross-section SEM images. For the thickness of gold lamellas and the distance between lamellas, a dedicated Python package (AQUAMI) is used on the cross section SEM images. More details about the software can be found elsewhere.[7,8] It is important to stress here that the pore size cannot be evaluated by AQUAMI due to a poor contrast on the plan view SEM images. (a) First, a zone is chosen on the

cross section SEM micrograph. (b) Then a black and white threshold of this zone is defined. The white region corresponds to the gold lamellas. The black part corresponds to the voids. (c) The software evaluates the transverse thickness of the gold lamellas and a Gaussian behavior can be observed. (d) As previously, the distance between lamella is evaluated and corresponds to a Gaussian distribution.

References

1 A.-A. El Mel, F. Boukli-Hacene, L. Molina-Luna, N. Bouts, A. Chauvin, D. Thiry, E. Gautron, N. Gautier and P.-Y. Tessier, *ACS Applied Materials & Interfaces*, 2015, **7**, 2310–2321.

2 L. H. Qian, A. Inoue and M. W. Chen, *Applied Physics Letters*, 2008, **92**, 093113.

3 E. Detsi, M. Salverda, P. R. Onck and J. Th. M. De Hosson, *Journal of Applied Physics*, 2014, **115**, 044308.

4 J. Huang, Y. Liu, X. He, C. Tang, K. Du and Z. He, *RSC Adv.*, 2017, **7**, 15747–15753.

5 R. C. Maher, in *Raman Spectroscopy for Nanomaterials Characterization*, ed. C. S. S. R. Kumar, Springer Berlin Heidelberg, Berlin, Heidelberg, 2012, pp. 215–260.

6 L. Qian, B. Das, Y. Li and Z. Yang, *Journal of Materials Chemistry*, 2010, **20**, 6891.

7 J. Stuckner, K. Frei, I. McCue, M. J. Demkowicz and M. Murayama, *Computational Materials Science*, 2017, **139**, 320–329.

8 I. McCue, J. Stuckner, M. Murayama and M. J. Demkowicz, *Scientific Reports*, 2018, **8**, 1–11.